

Noisy Pursuit and Pattern Formation of Self-Steering Active Particles

Segun Goh,^{1,*} Roland G. Winkler,^{1,†} and Gerhard Gompper^{1,‡}

¹*Theoretical Physics of Living Matter, Institute of Biological Information Processing, Forschungszentrum Jülich, 52425 Jülich, Germany*
(Dated: March 15, 2022)

We consider a moving target and an active pursuing agent, modeled as an intelligent active Brownian particle capable of sensing the instantaneous target location and adjust its direction of motion accordingly. An analytical and simulation study in two spatial dimensions reveals that pursuit performance depends on the interplay between self-propulsion, active reorientation, and random noise. Noise is found to have two opposing effects: (i) it is necessary to disturb regular, quasi-elliptical trajectories around the target, and (ii) slows down pursuit by increasing the traveled distance of the pursuer. We also propose a strategy to sort active pursuers according to their motility by circular target trajectories.

Motility is an essential source of pattern formation and collective dynamics in biological and artificial systems on scales from microbes, cells, and colloids, to microbots and animals [1–7]. Interacting active particles and agents exhibit fascinating collective behaviors, ranging from swarming of microorganisms [8–11] to lane-formation of ants [12, 13] and flocking of birds [14–17]. Theoretical models of such systems account for three main kinds of interactions in addition to self-propulsion, which are steric repulsion, velocity alignment, and hydrodynamics [1, 4, 18], where the latter implies a classification into dry and wet active matter. Simple stochastic models, like the active Brownian particle (ABP) and the run-and-tumble (RTB) model, have provided a theoretical framework for understanding dry active matter [3, 19].

Biological microorganisms differ in various important aspects from their active-colloid counterparts, which is their ability to sense their environment, to process the gathered information, and to steer their motion accordingly [20, 21]. The adopted response enables biological agents to perform goal-oriented motion, which includes cell motion in wound healing, foraging and prey-searching activities of animals, as well as traffic flows [22, 23] and pedestrian dynamics [24, 25] in social systems. Notwithstanding the apparent relevance of the role of information processing in motile systems, this has only very recently been started to be taken into account in studies of active matter [26–31]. Active adaptation should be distinguished from responses of particles in passive systems [32], whose dynamics is governed by conservative (reciprocal) interactions and external forces.

It is important to note that the process of information gathering can be non-reciprocal and long ranged, far beyond the range of standard colloidal interactions [33, 34]. A minimal cognitive flocking system has been introduced, which assumes that the moving entities navigate by using exclusively the instantaneous “visual information” they receive about the position of other entities [35, 36]. This includes systems and models, in which particles adjust their propulsion direction toward regions of highest particle concentration located inside the vision cone [35]. Alternatively, particle propulsion can be switched on or off depending on whether the particle number within the vision cone is above or below a threshold value [26–28]. Such vision-dependent propulsion mechanisms lead

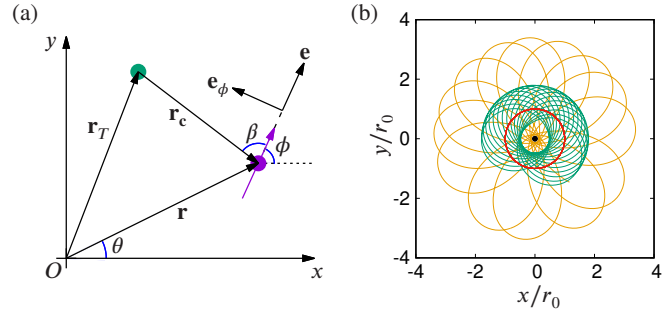


FIG. 1. (a) Schematics of the set-up for a stationary target located at \mathbf{r}_T (green bullet) and a pursuer at \mathbf{r} (purple bullet) with the propulsion direction \mathbf{e} (purple arrow), and the angle $\beta = \theta - \phi - \pi$. (b) Trajectories of pursuers in the absence of noise, with a stationary target at the origin (black bullet). The red circle represents the marginally stable fixed-point solution $(r, \beta) = (r_0, \pm\pi/2)$. Two rosette-like motions are shown for different initial conditions.

to particle aggregation and swarming without any attractive interactions.

In this study, we consider a minimal model of an intelligent active particle, which is capable of an active reorientation of its direction of motion toward a moving target. We employ the minimal cognitive active Brownian particle model introduced in Ref. [35], assuming perfect sensing, such that the pursuer always knows the exact location of the target. The success of the pursuer to approach and reach the target, which moves on a fixed, prescribed trajectory, depends on the relative velocities, the translational and rotational noise of the pursuer, and the strength of the reorientation force. In particular, orientational noise plays a fundamental role, as it is, on the one hand, necessary to reach a target, and, on the other hand, effectively slows down the pursuit by increasing the travel distance of the pursuer, and hence requires a larger pursuer velocity, compared to that of the target, for a successful pursuit. Furthermore, we demonstrate that a target moving on a circular trajectory can be used to localize pursuers, and to separate and sort them according to their velocities.

The translational motion of the intelligent active Brownian pursuer (iABP) is described by the overdamped Langevin

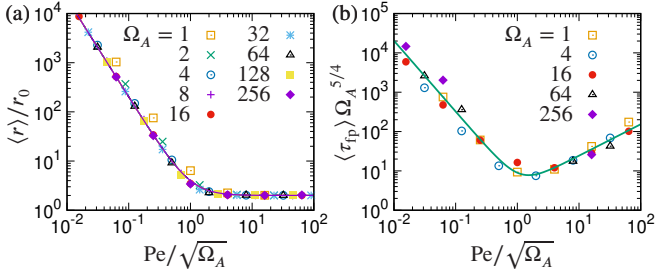


FIG. 2. (a) Mean distance of a pursuer from a stationary target as a function of the scaled Péclet number $Pe/\sqrt{\Omega_A}$ for various Ω_A . The line represents Eq. (8). (b) Mean first-passage times $\langle \tau_{fp} \rangle$ scaled by $\Omega_A^{-5/4}$ as a function of $Pe/\sqrt{\Omega_A}$ for various Ω_A . The solid line interpolates between the power-laws $\langle \tau_{fp} \rangle \sim Pe^{-9/5}$ for $Pe/\sqrt{\Omega_A} < 1$ and $\langle \tau_{fp} \rangle \sim Pe^{4/5}$ for $Pe/\sqrt{\Omega_A} > 1$.

equation [38, 39]

$$\dot{\mathbf{r}} = \mathbf{v} + \sqrt{2D_T} \boldsymbol{\eta}_T, \quad (1)$$

where $\boldsymbol{\eta}_T$ is a Gaussian white-noise stochastic process with zero mean and second moment $\langle \boldsymbol{\eta}_T(t) \cdot \boldsymbol{\eta}_T(t') \rangle = 2\delta(t-t')$, D_T is the translation diffusion coefficient, and $\mathbf{v} = v_0 \mathbf{e}$ is the active velocity of constant magnitude v_0 along the propulsion direction \mathbf{e} ($|\mathbf{e}| = 1$). The time evolution of $\mathbf{e}(t)$ is determined by orientational diffusion due to an active process or thermal fluctuations as for a standard ABP [3, 19], and an *active adaptation* contribution \mathbf{f}_A , hence,

$$\dot{\mathbf{e}} = \mathbf{f}_A + \sqrt{2D_R} \boldsymbol{\eta}_R \times \mathbf{e}, \quad (2)$$

with the Gaussian and Markovian stochastic process $\boldsymbol{\eta}_R$ of zero mean, the second moment $\langle \boldsymbol{\eta}_R(t) \cdot \boldsymbol{\eta}_R(t') \rangle = 2\delta(t-t')$, and the rotational diffusion coefficient D_R . The active contribution is $\mathbf{f}_A = -C_0 \mathbf{e} \times (\mathbf{e} \times \mathbf{r}_c / |\mathbf{r}_c|)$, where $\mathbf{r}_c = \mathbf{r} - \mathbf{r}_T$ is the vector connecting the pursuer at \mathbf{r} and the target at $\mathbf{r}_T(t)$. The adaptive force \mathbf{f}_A is orthogonal to \mathbf{e} and $\mathbf{f}_A = 0$ when \mathbf{e} is parallel to \mathbf{r}_c [35].

We consider a two-dimensional system and polar coordinates for \mathbf{r} and \mathbf{e} , as indicated in Fig. 1(a), and introduce dimensionless quantities by measuring length and time in units of $r_H = \sqrt{D_T/D_R}$, where r_H is analogous to the Stokes radius of a spherical colloid in a fluid, and D_R , respectively, which corresponds to $r \rightarrow r/r_H$ and $t \rightarrow D_R t$. The equations of motion then become

$$\dot{r} = Pe \cos(\theta - \phi) + \sqrt{2}\eta_r, \quad (3)$$

$$\dot{\theta} = -\frac{Pe}{r} \sin(\theta - \phi) + \frac{\sqrt{2}}{r} \eta_\theta, \quad (4)$$

$$\dot{\phi} = -\frac{\Omega_A}{r_c} (r \sin(\theta - \phi) - \mathbf{r}_T \cdot \mathbf{e}_\phi) + \sqrt{2}\eta_R, \quad (5)$$

with Péclet number Pe and active reorientation strength Ω_A ,

$$Pe = v_0 / (r_H D_R), \quad \Omega_A = C_0 / D_R, \quad (6)$$

the unit vector $\mathbf{e}_\phi = (-\sin \phi, \cos \phi)^T$, $r_c = |\mathbf{r} - \mathbf{r}_T|$, and the noise correlation functions $\langle \eta_\kappa(t) \eta_\kappa(t') \rangle = \delta(t-t')$, $\kappa \in \{r, \theta, R\}$. The active reorientation of the pursuer toward a target (Eq. (5)) is of the form of interactions applied in various other systems, e.g., the classical XY-model [40], Kuramoto oscillators [41], and minimal cognitive models in swarming [35].

We first consider the case where the pursuer moves much faster than the target, corresponding to the limit of a stationary target which we place at the origin of the reference system, i.e., $\mathbf{r}_T = 0$. In the noise-free limit, $Pe \gg 1$ and $\Omega_A \gg 1$, the stability analysis of Eqs. (3) - (5) yields the marginally stable fixed points (see Supplemental Material [37])

$$r_0 = Pe/\Omega_A, \quad \beta_0 = \theta_0 - \phi_0 - \pi = \pm\pi/2, \quad (7)$$

which corresponds to circular trajectories with the radius $r_0 = Pe/\Omega_A = r_H v_0 / C_0$ (red circle in Fig. 1(b)). Surprisingly, the fixed point conditions neither correspond to the solution where the pursuer is located at the target position, nor to a configuration where the pursuer is oriented toward the target. Notably, the circular trajectory emerges by the specific form of self-propulsion, in which the pursuer cannot stop and reorient, but moves with a constant magnitude v_0 of the velocity — as it is characteristic for ABPs. Numerically, quasi-periodic orbits are obtained, which “oscillate” around the circle of radius r_0 (Fig. 1(b)), depending on the initial conditions when $r \neq r_0$ —reminiscent of the planetary motion around the sun with perihelion rotation. Thus, without noise, the pursuer can never reach the target! Instead, noise is needed to kick the pursuer out of a quasi-periodic orbiting motion.

The presence of noise changes the pursuer dynamics qualitatively, with two distinct behaviors depending on the Péclet number. For $r_0 \ll 1$, i.e., $Pe \ll 1$, a pursuer preferentially aligns toward the target, and $\langle \cos \beta \rangle \lesssim 1$ for $\Omega_A \gg 1$, where $\beta = \theta - \phi - \pi$ is the supplementary angle to the angle $\theta - \phi$ between the vectors \mathbf{r} and \mathbf{e} (Supplemental Material, Movie S1 [37]). Then, the Fokker-Planck equation [42] for the radial distance yields the radial probability distribution function $P(r) \sim e^{-2r/\langle r \rangle}$ with the average radial distance $\langle r \rangle = 2/Pe$ (Supplemental Material [37]). In the opposite limit $Pe \gg 1$ and $\Omega_A \gg 1$, we again find an exponential distribution function for r , but now with the average $\langle r \rangle = 2r_0$. Here, a pursuer traverses rosette-like trajectories as in the noise-free limit, however, now perturbed by noise with an essentially uniform distribution of the angle β (Supplemental Material, Movie S2 [37]). The average radius of both dynamical regimes is well described by the expression

$$\bar{r} = 2r_0 (1 + 1/(r_0^2 \Omega_A)), \quad (8)$$

as shown in Fig. 2(a), which interpolates between the predicted limits. The minimum distance in terms of Pe and Ω_A follows for $Pe/\sqrt{\Omega_A} = 1$. This demonstrates that strong self-propulsion not necessarily enhances pursuit performance, but rather that magnitudes of propulsion and reorientation have to work in unison. Here, noise plays an important role, because $Pe/\sqrt{\Omega_A}$ depends on D_R .

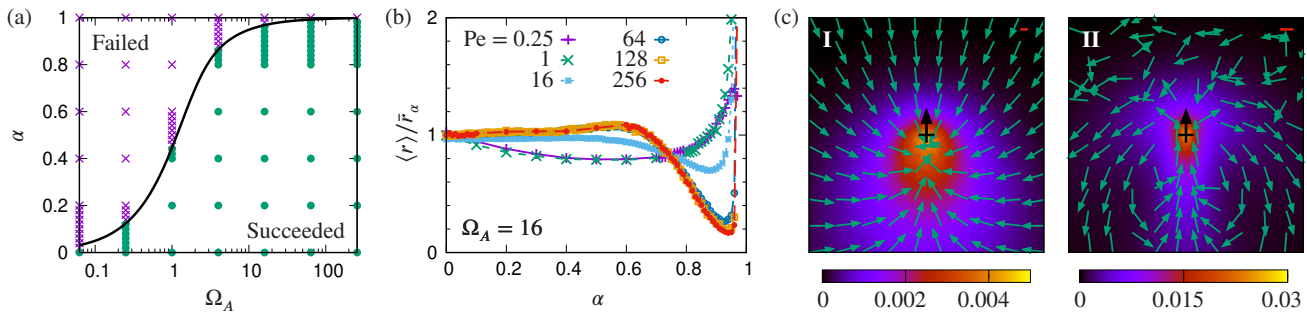


FIG. 3. (a) Phase diagram of the pursuit of a linearly moving target. Symbols indicate failed (\times) and successful (\bullet) pursuit. The Péclet number is $Pe = 16$ and the initial distance between the target and the pursuer is $r_{\text{mit}} = 10^5$. The black line depicts α_0 of Eq. (9). (b) Mean distance $\langle r \rangle$ between target and pursuer scaled by $\bar{r}_\alpha = 2Pe/\Omega_A[1 + \Omega_A/(Pe^2(1 - \alpha))]$ as a function of α for various Péclet numbers (symbols). The lines are guides for the eye. (c) Density distribution and orientation of the propulsion directions for $Pe = 0.25$ (I), $Pe = 64$ (II), $\alpha = 0.6$, and $\Omega_A = 16$. The target position is indicated by a plus (+) and the moving direction by an arrow. The red scale bars indicate the Stokes radius of the pursuers (cf. Supplemental Material, Movies S3 and S4 [37]).

To characterize the influence of noise further, a mean first-passage time [43] is calculated as the average time of a pursuer starting within a circle of radius of r_H centered at the target and returning for the first time again to the circle. Examples of the obtained probability distributions of return times are provided in the Supplemental Material [37]. The mean first-passage time τ_{fp} is then calculated as average of the return time starting at a shortest time, which is chosen as the time where the pursuer mean-square displacement exceeds the radius r_H . Figure 2(b) displays the mean first-passage time as a function of the Péclet number and various Ω_A . Interestingly, the τ_{fp} data for the various Pe and Ω_A all collapse onto an universal scaling curve when plotted as a function of the ratio $Pe/\sqrt{\Omega_A}$. The solid line in Fig. 2(b) presents a interpolation with the power-laws $\langle \tau_{\text{fp}} \rangle \sim Pe^{-9/5}$ for $Pe/\sqrt{\Omega_A} < 1$ and $\langle \tau_{\text{fp}} \rangle \sim Pe^{4/5}$ for $Pe/\sqrt{\Omega_A} > 1$. Consistent with the minimal mean pursuer-target distance for $Pe/\sqrt{\Omega_A} = 1$, the mean first-passage time is also minimal for the same value.

For moving targets, the pursuer dynamics changes qualitatively. We examine first the case, where the target moves along a straight line $\mathbf{r}_T = (u_0 t) \mathbf{e}_y$ with constant velocity u_0 . The pursuer position is characterized in a co-moving reference frame of the target, i.e., $\mathbf{r}_T \equiv 0$ and $\mathbf{r} \equiv \mathbf{r}_c$. The fixed point of the noise-free equations of motion is then $\theta = -\pi/2$ and $\phi = \pi/2$, i.e., $\beta = 0$ and the pursuer points directly toward the target (Supplemental Material [37]). The pursuer follows the target at a constant distance when the velocity ratio $\alpha = u_0/v_0$ is unity. Similarly, in the absence of noise, the pursuer follows the target as long as $\alpha < 1$ along initial-condition dependent trajectories, comparable to a stationary target. In contrast, for $\alpha > 1$ the distance between target and pursuer diverges and pursuit fails, both with and without noise.

A ratio $\alpha < 1$ is particularly important in the presence of noise, because then a pursuer trajectory can never be as straight as the target trajectory, so that a speed $v_0 > u_0$ is required to reduce the distance to the target at large distance ($r \gg 1$). In the limit $r/r_0 \gg 1$, the dynamics of the iABP propulsion

direction, ϕ , decouples from that of the iABP position, and we find

$$\langle \cos \beta \rangle = I_1(\Omega_A)/I_0(\Omega_A) \equiv \alpha_0(\Omega_A), \quad (9)$$

where $I_0(\Omega_A)$ and $I_1(\Omega_A)$ are modified Bessel functions of the first kind (Supplemental Material, Sec. S-II A [37]). The equation of motion for the radial distance leads then to the condition $\alpha < \alpha_0(\Omega_A)$ for a successful pursuit, which is confirmed by our simulations as shown in Fig. 3(a). Here, the dynamical behavior for small $Pe \ll 1$ is very similar to that of a stationary target, with an exponential distribution of the distance r , but with the mean value $\langle r \rangle = 2/[Pe(1 - \alpha)]$. In particular for $\Omega_A \gg 1$, $\alpha_0 \lesssim 1$ and the pursuer is preferentially orientated toward the target (Fig. 3(c)-I).

In the limit of large $Pe \gg 1$, the pursuer overshoots the target, specifically for $\alpha \ll 1$ (Fig. 3(c)-II). As for a stationary target, we find an exponential distribution of the radial distance with $\langle r \rangle = 2r_0$. Overall, the mean distance is well described by the expression $\bar{r}_\alpha = 2Pe/\Omega_A[1 + \Omega_A/(Pe^2(1 - \alpha))]$ as long as $\alpha \lesssim 0.7$ (Fig. 3(b)), with the additional dependence on α compared to Eq. (8) (see also Supplemental Material, Fig. S5(a) [37]). For $\alpha \gtrsim 0.7$ and $Pe \gtrsim 10$, we find substantial deviations from \bar{r}_α , and $\langle r \rangle$ assumes a minimum in the vicinity of α_0 before it diverges in the limit $\alpha \rightarrow 1$. Configurations for α values in the vicinity of the minimum are similar to those at the fixed point, $\alpha = 1$, yet with $\alpha < 1$ due to noise (Supplemental Material, Movie S5 [37]).

Lastly, we explore the role of the shape of the target trajectory on pursuit by studying a target moving on a circular trajectory with angular velocity ω_T and the radius r_T , i.e., $\mathbf{r}_T = r_T(\cos(\omega_T t), \sin(\omega_T t))^T$. The noise-free equations of motion yield a stable fixed point with the angle $\beta = \pi/2$ and characteristic pursuer radius $\bar{r} = Pe/\omega_T$ (Supplemental Material [37]). Again, the dynamics depends on the ratio of the target and pursuer velocity $\alpha = u_0/v_0 = r_T\omega_T/v_0 = r_T/\bar{r}$, with the target velocity $u_0 = \omega_T r_T$. In the limit of $\alpha \ll 1$, the pursuer radius is much larger than the target radius, and the equations of motion reduce again to those of a fixed target.

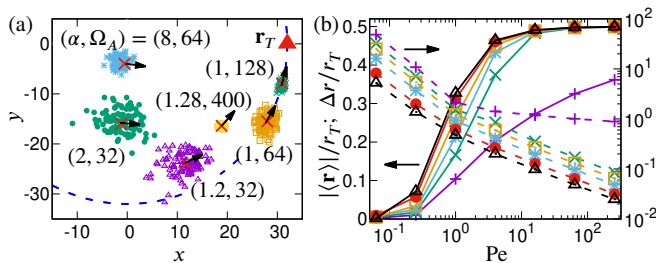


FIG. 4. Target on circular trajectory. (a) Groups of pursuers moving on circles following the target located at $\mathbf{r}_T = (32, 0)^T$ (red triangle) in a co-rotating reference frame with origin at $(0, 0)$ for various pairs (α, Ω_A) , $u_0/(r_H D_R) = 512$, and $\omega_T = 16$. The dashed line illustrates the circle for $\alpha = 1$. The black arrows indicate the average moving direction of a group, and the red crosses the theoretical prediction Eq. (S21) (cf. Supplemental Material, Movies S6, S7, and S8 [37]). (b) Mean distance (left axis) and the root-mean square fluctuations (right axis) as a function of the Péclet number for various target radii: $r_T = 2$ (+), 3 (x), 4 (□), 6 (*), 12 (●), and 20 (△). Here, $r_0 = 1$ and $\alpha = 2$.

For $\alpha > 1$, the target moves faster than the pursuer. However, the distance r_c does not diverge, because of the target’s circular trajectory. Pursuers are able to keep track, but in a strikingly different manner from straight moving targets. Since $\alpha = r_T/\tilde{r} > 1$, pursuers are located inside the circle of the target trajectory, where they move shorter distances than the target and, hence, are able to remain close to it. As the fixed point is stable, pursuers are localization in its vicinity and move on circles with a mean radius $\tilde{r} = r_T/\alpha$, only perturbed by noise (Supplemental Material, Sec. S-1 C [37]). This is confirmed by our simulations and, as depicted in Fig. 4(a), the fixed-point prediction describes the pursuit dynamics very well. The increasing influence of noise for $Pe < 1$ causes deviations from the analytical prediction, in particular for small r_T (Supplemental Material, Fig. S1(b)). The mean position is shifted toward the origin of the target circle as noise becomes more important, which allows pursuers to reduce the path length and to follow the target. Still, accumulation of slow pursuers inside the target circle is robustly observed in simulations. In addition, the fixed point analysis predicts a phase shift between the instantaneous target angle $\omega_T t$ and the pursuer angle $\theta(t)$, which depends on α and the ratio Ω_A/ω_T . This is demonstrated in Fig. 4(a), which shows a decreasing shift with increasing Ω_A at a given α , consistent with the theoretical expression (Supplemental Material, Sec. S-1 C [37]).

Noise also affects the distribution of particles in a group of non-interacting pursuers around their mean position, and leads to a radial repositioning of iABPs with respect to the radius \tilde{r} during their circular motion. This is similar to repositioning of birds in a flock during a turn, and is a consequence of the nearly constant pursuer speed, which implies a comparable length and curvature of the traveled paths of the iABPs [44]. As a consequence, a clockwise rotation of the pursuers’ propulsion direction occurs in a reference frame rotating counterclockwise with the frequency ω_T (Supplemental Material,

Fig. S1(d) and Movie S8 [37]).

Figure 4(b) emphasizes the influence of noise on the mean radius $|\langle \mathbf{r} \rangle|$ of a group of (noninteracting) pursuers for various target radii and Péclet numbers for $r_0 = 1$ and $\alpha = 2$. Here, $|\langle \mathbf{r} \rangle|$ is the radius of the center-of-mass position $\langle \mathbf{r} \rangle$ of the pursuer group. Due to noise, the mean radius is very small in the limit $Pe \rightarrow 0$, but increase with increasing Pe and saturates at the noise-free, large Péclet-number limit $\langle r \rangle = \tilde{r} = r_T/\alpha = 1/2$ for the considered α . The convergence toward the limit cycle of the noise-free case with increasing Pe is reflected in the root-mean-square fluctuations Δr with respect to $|\langle \mathbf{r} \rangle|$, which exceed $|\langle \mathbf{r} \rangle|$ by far for $Pe < 1$ and decrease with increasing Pe .

As our studies show, targets moving on circular trajectories can be employed for pattern formation and particle sorting according to the propulsion strength and reorientation capability. This can be seen as an “inverse herding” effect, where a fast-moving circling sheep keeps a herd of slower shepherd dogs together, which are all chasing the sheep.

In summary, we have considered noisy pursuit dynamics of iABPs, for various types of target trajectories. We have shown that noise plays a dual role in the successful approach of the target. On the one hand, it is required to kick the pursuers out of regular, quasi-period orbits around the target, and thus facilitates target approach. On the other hand, noisy trajectories are longer than straight trajectories, and, hence, slow down the pursuit, requiring higher pursuer velocities. Finally, we have demonstrated that the geometry of target trajectories can be employed for pattern formation and sorting of active agents according to their motility.

* s.goh@fz-juelich.de

† r.winkler@fz-juelich.de

‡ g.gompper@fz-juelich.de

- [1] E. Lauga and T. R. Powers, The hydrodynamics of swimming microorganisms, *Rep. Prog. Phys.* **72**, 096601 (2009).
- [2] T. Vicsek and A. Zafeiris, Collective motion, *Phys. Rep.* **517**, 71 (2012).
- [3] C. Bechinger, R. Di Leonardo, H. Löwen, C. Reichardt, G. Volpe, and G. Volpe, Active particles in complex and crowded environments, *Rev. Mod. Phys.* **88**, 045006 (2016).
- [4] J. Elgeti, R. G. Winkler, and G. Gompper, Physics of microswimmers—single particle motion and collective behavior: a review, *Rep. Prog. Phys.* **78**, 056601 (2015).
- [5] S. Palagi and P. Fischer, Bioinspired microrobots, *Nat. Rev. Mater.* **3**, 113 (2018).
- [6] G. Gompper *et al.*, The 2020 motile active matter roadmap, *J. Phys.: Condens. Matter* **32**, 193001 (2020).
- [7] M. R. Shaebani, A. Wysocki, R. G. Winkler, G. Gompper, and H. Rieger, Computational models for active matter, *Nat. Rev. Phys.* **2**, 181 (2020).
- [8] D. B. Kearns, A field guide to bacterial swarming motility, *Nat. Rev. Microbiol.* **8**, 634 (2010).
- [9] A. Sokolov and I. S. Aranson, Physical properties of collective motion in suspensions of bacteria, *Phys. Rev. Lett.* **109**, 248109 (2012).

- [10] H. H. Wensink, J. Dunkel, S. Heidenreich, K. Drescher, R. E. Goldstein, H. Löwen, and J. M. Yeomans, Meso-scale turbulence in living fluids, *Proc. Natl. Acad. Sci. USA* **109**, 14308 (2012).
- [11] K. Qi, E. Westphal, G. Gompper, and R. G. Winkler, Emergence of active turbulence in microswimmer suspensions due to active hydrodynamic stress and volume exclusion, *Commun. Phys.* accepted for publication (2022).
- [12] I. D. Couzin and N. R. Franks, Self-organized lane formation and optimized traffic flow in army ants, *Proc. R. Soc. B* **270**, 139 (2003).
- [13] O. Ayalon, Y. Sternklar, E. Fonio, A. Korman, N. S. Gov, and O. Feinerman, Sequential decision-making in ants and implications to the evidence accumulation decision model, *Front. Appl. Math. Stat.* **7**, 37 (2021).
- [14] A. Cavagna and I. Giardina, Bird flocks as condensed matter, *Annu. Rev. Condens. Matter Phys.* **5**, 183 (2014).
- [15] G. Popkin, The physics of life, *Nature* **529**, 16 (2016).
- [16] T. Vicsek, A. Czirók, E. Ben-Jacob, I. Cohen, and O. Shochet, Novel type of phase transition in a system of self-driven particles, *Phys. Rev. Lett.* **75**, 1226 (1995).
- [17] J. Toner and Y. Tu, Long-range order in a two-dimensional dynamical xy model: How birds fly together, *Phys. Rev. Lett.* **75**, 4326 (1995).
- [18] E. M. Purcell, Life at low reynolds number, *Am. J. Phys.* **45**, 3 (1977).
- [19] M. E. Cates and J. Tailleur, Motility-induced phase separation, *Annu. Rev. Condens. Matter Phys.* **6**, 219 (2015).
- [20] J. F. Jikeli, L. Alvarez, B. M. Friedrich, L. G. Wilson, R. Pascal, R. Colin, M. Pichlo, A. Rennhack, C. Brenker, and U. B. Kaupp, Sperm navigation along helical paths in 3d chemoattractant landscapes, *Nat. Commun.* **6**, 7985 (2015).
- [21] R. Harpaz, M. N. Nguyen, A. Bahl, and F. Engert, Precise visuomotor transformations underlying collective behavior in larval zebrafish, *Nat. Commun.* **12**, 6578 (2021).
- [22] D. C. Gazis, Mathematical theory of automobile traffic, *Science* **157**, 273 (1967).
- [23] D. Chowdhury, L. Santen, and A. Schadschneider, Statistical physics of vehicular traffic and some related systems, *Phys. Rep.* **329**, 199 (2000).
- [24] A. Seyfried, B. Steffen, W. Klingsch, and M. Boltes, The fundamental diagram of pedestrian movement revisited, *J. Stat. Mech. Theory Exp.* **2005**, P10002 (2005).
- [25] M. Moussaïd, D. Helbing, and G. Theraulaz, How simple rules determine pedestrian behavior and crowd disasters, *Proc. Natl. Acad. Sci. USA* **108**, 6884 (2011).
- [26] T. Bäuerle, A. Fischer, T. Speck, and C. Bechinger, Self-organization of active particles by quorum sensing rules, *Nat. Commun.* **9**, 3232 (2018).
- [27] F. A. Lavergne, H. Wendehenne, T. Bäuerle, and C. Bechinger, Group formation and cohesion of active particles with visual perception-dependent motility, *Science* **364**, 70 (2019).
- [28] B. Qian, D. Montiel, A. Bregulla, F. Cichos, and H. Yang, Harnessing thermal fluctuations for purposeful activities: the manipulation of single micro-swimmers by adaptive photon nudging, *Chem. Sci.* **4**, 1420 (2013).
- [29] D. Levis, A. Diaz-Guilera, I. Pagonabarraga, and M. Starnini, Flocking-enhanced social contagion, *Phys. Rev. Research* **2**, 032056 (2020).
- [30] J. Zhang, R. Alert, J. Yan, N. S. Wingreen, and S. Granick, Active phase separation by turning towards regions of higher density, *Nat. Phys.* 10.1038/s41567-021-01238-8 (2021).
- [31] L. Alvarez, M. A. Fernandez-Rodriguez, A. Alegria, S. Arrese-Igor, K. Zhao, M. Kröger, and L. Isa, Reconfigurable artificial microswimmers with internal feedback, *Nat. Commun.* **12**, 4762 (2021).
- [32] C. Kaspar, B. J. Ravoo, W. G. van der Wiel, S. V. Wegner, and W. H. P. Pernice, The rise of intelligent matter, *Nature* **594**, 345 (2021).
- [33] S. Saha, J. Agudo-Canalejo, and R. Golestanian, Scalar active mixtures: The nonreciprocal cahn-hilliard model, *Phys. Rev. X* **10**, 041009 (2020).
- [34] M. Fruchart, R. Hanai, P. B. Littlewood, and V. Vitelli, Non-reciprocal phase transitions, *Nature* **592**, 363 (2021).
- [35] L. Barberis and F. Peruani, Large-scale patterns in a minimal cognitive flocking model: Incidental leaders, nematic patterns, and aggregates, *Phys. Rev. Lett.* **117**, 248001 (2016).
- [36] R. Bastien and P. Romanczuk, A model of collective behavior based purely on vision, *Sci. Adv.* **6**, eaay0792 (2020).
- [37] See Supplemental Material at [URL will be inserted by publisher] for analytical calculations, further simulation results, and movies.
- [38] E. Fodor, C. Nardini, M. E. Cates, J. Tailleur, P. Visco, and F. van Wijland, How far from equilibrium is active matter?, *Phys. Rev. Lett.* **117**, 038103 (2016).
- [39] S. Das, G. Gompper, and R. G. Winkler, Confined active brownian particles: theoretical description of propulsion-induced accumulation, *New J. Phys.* **20**, 015001 (2018).
- [40] J. M. Kosterlitz and D. J. Thouless, Ordering, metastability and phase transitions in two-dimensional systems, *J. Phys. C: Solid State Phys.* **6**, 1181 (1973).
- [41] J. A. Acebrón, L. L. Bonilla, C. J. Pérez Vicente, F. Ritort, and R. Spigler, The Kuramoto model: A simple paradigm for synchronization phenomena, *Rev. Mod. Phys.* **77**, 137 (2005).
- [42] H. Risken, *Fokker-Planck equation: methods of solution and applications* (Springer-Verlag, Berlin, 1989).
- [43] S. Redner, *A guide to first-passage processes* (Cambridge university press, Cambridge, 2001).
- [44] C. K. Hemelrijk and H. Hildenbrandt, Some causes of the variable shape of flocks of birds, *PLoS one* **6**, e22479 (2011).